# Representability and Dynamical Consistency in Coarse-Grained Models

Manuel Palma Banos,† Alexander V. Popov,† and Rigoberto Hernandez\*,†,‡,¶

†Department of Chemistry, Johns Hopkins University, Baltimore, Maryland 21218, USA

‡Department of Chemical & Biomolecular Engineering, Johns Hopkins University,

Baltimore, Maryland 21218, USA

¶Department of Materials Science & Engineering, Johns Hopkins University, Baltimore,

Maryland 21218, USA

E-mail: r.hernandez@jhu.edu

#### Abstract

We address the challenge of representativity and dynamical consistency when unbonded fine-grained particles are collected together into coarse-grained particles. We implement a hybrid procedure for identifying and tracking the underlying fine-grained particles—e.g., atoms or molecules—by exchanging them between the coarse-grained particles periodically at a characteristic time. The exchange involves a back-mapping of the coarse-grained particles into fine-grained particles, and a subsequent reassignment to coarse-grained particles conserving total mass and momentum. We find that an appropriate choice of the characteristic exchange time can lead to the correct effective diffusion rate of the fine-grained particles when simulated in hybrid coarse-grained dynamics. In the compressed (supercritical) fluid regime, without the exchange term, fine-grained particles remain associated to a given coarse-grained particle, leading to substantially lower diffusion rates than seen in all-atom molecular dynamics of the finegrained particles. Thus, this work confirms the need for addressing the representativity of fine-grained particles within coarse-grained particles, and offers a simple exchange mechanism so as to retain dynamical consistency between the fine- and coarse- grained scales.

#### 1 Introduction

The effective acceleration of coarse-grained (CG) particles relative to the underlying fine-grained (FG) particles has been widely reported, <sup>1–14</sup> and includes solvents such as polymers <sup>2,4,5,9</sup> and water. <sup>10,11,13,14</sup> It is a consequence of the loss of the fast motion of the "smaller" particles, and it is often seen as an advantage because the integration time step can be increased to reduce the computational cost. In order to match observables, however, the time scales must be corrected in some way. In coarse graining a Janus particle system, <sup>12</sup> we found earlier that the usual one-parameter time scale rescaling <sup>4,5,9</sup> to match the diffusion rate of the CG particles to those of the FG particles did not lead to the correct dynamics in the correlation function for other observables. Dynamical consistency for some of these other observables, however, were retained if the dynamics was rescaled by applying Langevin friction. <sup>1,3,6,12</sup> One emerging route for accounting for the excess entropy difference between the FG and CG representations is the fluctuation matching approach recently introduced by Jin et al. <sup>13,14</sup> Nevertheless, the need for alternative approaches <sup>1,3-6,9,15</sup> retaining dynamical consistency between the FG and CG scales remains. <sup>12,16,17</sup>

In dissipative particle dynamics (DPD), <sup>2,18,19</sup> for example, the CG particles—of appropriate dimensions—interact through appropriately renormalized potentials while experiencing dissipation and stochastic accelerations as a consequence of the untracked FG degrees of freedom. This model, as many others, is challenged with the question of transferability in ensuring that the forms (or parameters) of the potential and dissipative terms are retained between different systems at varying scales. Nevertheless, this challenge of transferability can often be addressed using characteristic inter-particle terms for chosen groups, and has been seen to be effective in a number of applications. <sup>4,20–23</sup>

A second challenge involves the representation of FG particles within a particular CG particle. <sup>24–26</sup> By naïvely associating many FG particles to a single dissipative entity —CG particle— the many degrees of freedom associated with the FG motion are lost. This leads to substantial discrepancies when comparing the predicted thermodynamic quantities of the CG

systems with that of the FG system. <sup>4,20,22,24,27</sup> Here, we recognize that this representability problem can be exacerbated by the fact that the selection or association of a particular set of FG particles to a given CG particle remains fixed throughout the simulation. This can lead to additional errors in the spread of the FG particles, and the dynamics of the CG particles. Thus, the aim of this work is to address the role of representability—as defined here—in dynamical consistency.

For example, in the context of water solvents, the issue of association in representability does not arise if the water is treated as a uniform solvent, or if only one water molecule is associated with each CG particle, because all of the water molecules are treated on the same footing. However, for a CG solvent in which each particle represents a finite number of multiple water molecules, the water molecules in each bead are forever tied together though in a real system they would not be. This example can be generalized to any kind of mesoscopic coarse graining of a solvent in which a group of particles or atoms which are not bonded to each other are associated with a single CG particle. Therein, the motion of the FG particles is usually limited to remain associated with its CG particle during the entirely of the simulation. While the CG particles may effectively accelerate, as described above, the underlying FG particle is effectively decelerated because it cannot diffuse relative to its associated CG particle. The resulting time scales of the FG particles is therefore affected by this competition of accelerating and decelerating mechanisms, and will certainly not be corrected by the naive rescaling of time typically used to correct only the acceleration of the CG particle. At the coarse-grained level, the problem is that the composition of a given CG particle changes with time as the FG particles move between them. In this work, we demonstrate that this FG mechanism affects the observables of the CG simulations, and thus an accounting for exchange—that is association—in representability is needed to ensure dynamical consistency in coarse-grained simulations. We also introduce a mechanism for the periodic exchange of the FG particles between CG particles at a frequency that is characteristic of the diffusive escape from the CG particles. We demonstrate this approach to resolve the dynamics in a coarse-grained model of a supercritical argon fluid which we chose because of the earlier success in mesoscopic coarse-graining Lennard-Jones (LJ) fluids reported by Voth and coworkers.<sup>28</sup>

The current paper is organized as follows. Section 2 describes the physical system under investigation. We then describe two algorithms for addressing the exchange problem in the CG representation of the FG particles. In Sections 3.3 and 3.4. In both algorithms, the system is periodically back-mapped (at a characteristic exchange time  $\Delta t$ ), to diffused FG particle positions and then coarse-grained into re-associated CG particles. Tuning  $\Delta t$  allows us to equate the apparent diffusion of FG particles in this hybrid system to that of the all atom (AA) simulations. A discussion of our results and conclusion are provided in Sections 4 and 5, respectively.

# 2 Methods: System

The methodology to be presented below is relevant to any FG system that is coarse-grained to include unbonded particles within a given coarse-grained particle. For illustration, we chose the FG system to be either a hard sphere (HS) or a LJ gas as such gases have served as typical examples in considering fluids at different scales. <sup>19,28,29</sup> As detailed in Subsec. 2.1, we use the particular parameters for argon although the results do not depend on this specification. In Subsec. 2.2, we provide details of the selected procedures for constructing CG particles that include—ipso facto—multiple unbonded argon atoms.

# 2.1 Fine-grained system

The chosen system consists of LJ particles representing argon atoms at temperature T, each having mass  $m_0 = 39.95$  a.u., and interacting through a specified potential. The atoms are immersed in a box with the side length L. The temperature and side length are sampled at the values: T = 270, 300 and 330 K, and L = 40, 42.5 and 45 Å.

We explore the behavior of the argon system when the pair potential between argon atoms is characterized by either of two typical choices: (i) the HS case<sup>30</sup> with the spherical diameter set to  $\sigma = 3.5$  Å, and (ii) the soft sphere case where the interaction between the atoms is described by a LJ potential, <sup>30,31</sup>

$$U_{\rm Ar}(r) = 4 \,\epsilon_0 \left[ \left( \frac{\sigma}{r} \right)^{12} - \left( \frac{\sigma}{r} \right)^6 \right] \Theta(r_{\rm cut} - r) \,, \tag{1}$$

with  $\epsilon_0 = 0.238$  kcal/mol,  $\sigma = 3.5$  Å and  $r_{\rm cut} = 3 \sigma$ .  $\Theta(x)$  is the usual Heaviside step function which goes from 0 to 1 at the origin.

We found that placing N = 1000 particles in a periodic box was sufficient to converge the behavior of the reported variables. Given the value of  $\sigma$  and the three selected box lengths specified above, the volume fractions,

$$\phi = N \frac{\pi}{6} \frac{\sigma^3}{L^3},\tag{2}$$

correspond to  $\phi = 0.351$ , 0.292 and 0.246. All three cases are well below the maximum packing fraction (0.740), but also well within the supercritical regime at the specified temperature.<sup>32–34</sup>

### 2.2 Coarse-grained system

Performing a mesoscopic coarse-graining, we specify the masses and interaction potentials of the CG structures similarly to the approach in Refs. 21 and 28. For the specific details of the current implementation, refer to Sections 3.3.2 and 3.4.2. We treat all the FG particles within a specific CG structure equally and inclusively, i.e., their masses and momenta are not shared between several CG cells.

We start with the CG potential of mean force (PMF)

$$U(\hat{\mathbf{R}}) = -\beta^{-1} \ln \int d\hat{\mathbf{r}} \exp(-\beta u(\hat{\mathbf{r}})) \, \delta(\hat{\mathcal{R}}(\hat{\mathbf{r}}) - \hat{\mathbf{R}}), \qquad (3)$$

where  $u(\hat{\mathbf{r}})$  is the total potential energy defined as

$$u(\hat{\mathbf{r}}) = \frac{1}{2} \sum_{i \neq j} U_{\text{Ar}}(\mathbf{r}_i - \mathbf{r}_j), \qquad (4)$$

 $\hat{\mathbf{R}} \equiv \{\mathbf{R}_1, \mathbf{R}_2, ...\}$  is the position vector of the CG particles,  $\hat{\mathbf{r}} \equiv \{\mathbf{r}_1, \mathbf{r}_2, ...\}$  is the position vector of the FG coordinates,  $\hat{\mathcal{R}}(\hat{\mathbf{r}}) \to \hat{\mathbf{R}}$  is the mapping between the FG and CG systems and  $\beta^{-1} = k_{\rm B}T$ .

The resulting CG forces are <sup>21</sup>

$$\mathbf{F}_{K}(\hat{\mathbf{R}}) = -\frac{\partial U(\hat{\mathbf{R}})}{\partial \mathbf{R}_{K}} = \left\langle \sum_{i \in S_{K}} \mathbf{f}_{i}(\hat{\mathbf{r}}) \right\rangle_{\hat{\mathbf{R}}}, \tag{5}$$

where  $\mathbf{f}_i(\hat{\mathbf{r}}) = -\partial u(\hat{\mathbf{r}})/\partial \mathbf{r}_i$ ,  $S_K$  is the set of FG particles belonging to the K-th CG cell, (Note that the upper-case indices refer to CG, while the lower-case indices refer to FG particles.) The angular brackets (constrained by  $\hat{\mathbf{R}}$ ) denote the Boltzmann average over the FG variables. and each averaged force resolves as

$$\langle \mathbf{f}_i(\hat{\mathbf{r}}) \rangle_{\hat{\mathbf{R}}} = \frac{\int d\hat{\mathbf{r}} \exp(-\beta u(\hat{\mathbf{r}})) \, \delta(\hat{\mathcal{R}}(\hat{\mathbf{r}}) - \hat{\mathbf{R}}) \, \mathbf{f}_i(\hat{\mathbf{r}})}{\int d\hat{\mathbf{r}} \exp(-\beta u(\hat{\mathbf{r}})) \, \delta(\hat{\mathcal{R}}(\hat{\mathbf{r}}) - \hat{\mathbf{R}})}.$$
 (6)

The dimensionality of the sum in the RHS of Eq. (5) depends on the number of FG particles pertaining to the K-th CG cell as listed in the set  $S_K$ . Its value depends on the ensemble average of their spatial configuration which can be characterized collectively by the occupied volume of the CG structure.

In addition to two-body interactions, Eq. (5) can contain three or more body terms.<sup>23</sup> Using an assumption that the largest forces arise from the surfaces of the CG structures, we neglect all higher order terms (as usual) and approximate the forces through a pairwise additive interaction:

$$\mathbf{F}_K(\hat{\mathbf{R}}) \approx \sum_{I \neq K} \mathbf{F}_{K,I} (\mathbf{R}_K - \mathbf{R}_I) .$$
 (7)

In turn, Eq. (5) can be integrated to give the PMF in an additive form:

$$U(\hat{\mathbf{R}}) \approx \frac{1}{2} \sum_{I \neq K} U_{K,I} (\mathbf{R}_K - \mathbf{R}_I).$$
 (8)

In the usual implementations, the sets  $S_K$  are independent of time and so the nature of the corresponding CG particle is similar. In what follows,  $S_K$  will be allowed to vary as the underlying FG particles can exchange their respective association. Interestingly, this change does not affect the form of the expression in Eq. (8) because the approximations that have led to it do not require them to be independent of time as should be clear from the pedantic derivation included here.

We assume that CG particles are spheres for which we adopt a WCA<sup>35</sup>-like potential energy (PE). For CG particles K and I with radii  $\rho_K$  and  $\rho_I$ , respectively, this interaction takes the form,

$$U_{K,I}(r) = \left(4\epsilon \left[ \left(\frac{\sigma_{K,I}}{r}\right)^{12} - \left(\frac{\sigma_{K,I}}{r}\right)^{6} \right] + \epsilon \right) \Theta(r_{K,I} - r),$$
(9)

where  $\sigma_{K,I} = \rho_K + \rho_I$  is the "diameter of interaction" between the CG particles. This function is truncated at the energy minimum  $r_{K,I} = 2^{1/6}\sigma_{K,I}$  thus including only the repulsive part. The energy parameter defining the steepness of the PE is chosen to be  $\epsilon = 10$  kcal/mol, and this is large enough that the CG system behaves almost like a HS gas. This choice for the PE, though facilitating the dynamics, may not be in agreement with a full bottom-up construction. For example, Voth and coworkers <sup>19,28</sup> reported effective potentials calculated from the bottom-up coarse-graining that are much softer, and may have different effects on the motion. However, the specific choice of PE should not change the need for consideration of the exchange of FG particles between CG particles which is the major result reported below.

Since no FG particle is involved in the definition of more than one CG structure, the

mass of the K-th CG particle consisting of  $N_K$  FG particles is simply  $^{21,36,37}$ 

$$M_K = N_K m_0 (10)$$

Similarly, the instantaneous momentum of the K-th CG particle is the sum of the instantaneous momenta of the FG particles in the set  $S_K$ . The specification of the mass in Eq. (10) allows us to specify its velocity.

# 3 Methods: Including Exchange in Coarse-Grained Dynamics

Determining the diffusion of FG particles in a CG model is challenging because CG particles have necessarily averaged away the information of the particles they contain. However, we can at least retain the identity of the FG particles associated with a given CG particle, and use that to observe the exchange—that is, the effective diffusion—of FG particles across the CG particles. The need for this kind of mechanism is reminiscent of that for the diffusion of a hydronium ion in water which we would not be able to capture if we were to restrict the excess charge to forever remain on a single CG hydronium particle. <sup>38,39</sup> In order to track the motion of the FG particles and address its representability, we introduce two possible ad hoc mechanisms described below. In Scheme 1, we exchange the FG particles between the CG particles at the cost of restructuring the entire system into an ordered array at periodic intervals on some effective exchange time. In Scheme 2, using the theoretical FG diffusion constant we modify the exchange between CG particles at their instantaneous positions rather than reassigning them to an ordered array.

#### 3.1 Initialization

We first prepare an equilibrated CG structure bottom-up by propagating an NVT AA system from an initial uniform array until it equilibrates. We found 10 picoseconds to be sufficient to obtain the necessary thermodynamic parameters for the CG calculations reported here. The coordinates (trajectories) of the particles and the pressure P measured numerically for it (Figure 1) serve as the initial configuration. The equilibrated AA trajectories are also used to determine the diffusion coefficient D at the FG scale; cf. Figure 2.

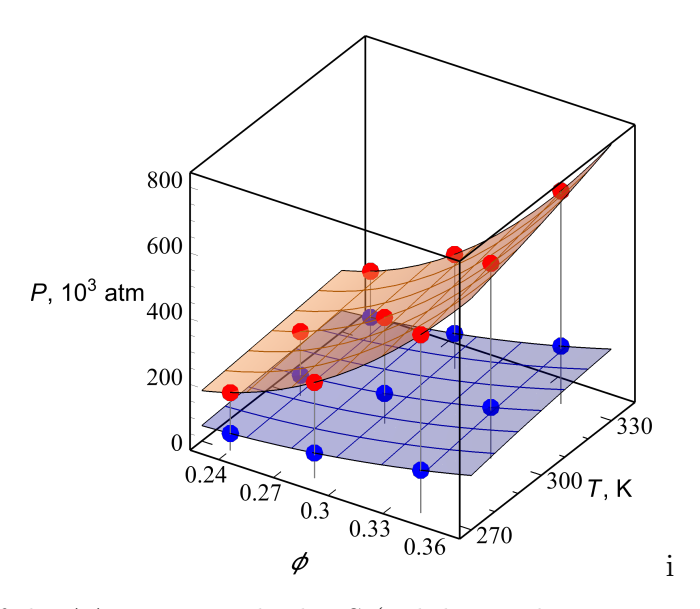


Figure 1: Pressure of the AA systems —both HS (red dots and orange interpolating surface) and LJ (blue dots and light blue surface)— at different temperatures and volume fractions.

A given initial FG structure is coarse-grained into roughly  $N_{\rm cg}$  CG particles which are placed uniformly in a rectilinear array within a periodic box as described in more detail in Sec. 3.3.2. The Voronoi tessellation  $^{36,37,40}$  of such ordered CG particles results in Voronoi polyhedra that are all cubic cells. Each FG particle is contained in one such cubic cell and associates to the CG particle at its center. (Note that, in the end, there may be fewer than  $N_{\rm cg}$  CG particles because some such particles may not have any FG particles inside their associated Voronoi cell.) Similarly, the masses of resulting initial array of CG particles will vary as they will each be proportional to the number of FG particles that they contain.

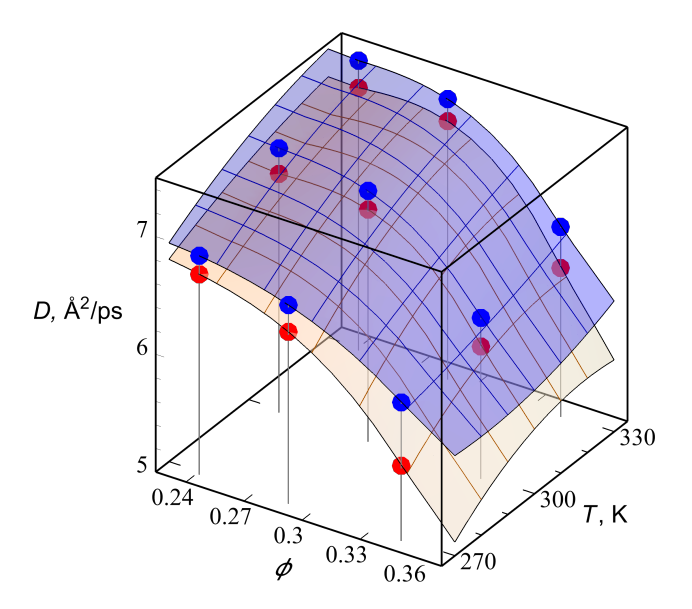


Figure 2: Diffusion coefficients of the AA systems – both HS and LJ – at different temperatures and volume fractions. The color scheme is the same as in Fig. 1.

If the FG particles are not exchanged during a simulation, then CG dynamics could be performed following the usual propagation procedure described in Subsec. 3.2 for the entire run. Schemes 1 and 2 describe two possible procedures for propagating the CG dynamics with periodic exchanges of FG particles. The comparison of the long-time diffusion constant and other observables in 4 reveals the effect of including the exchange term.

# 3.2 CG Dynamics

The CG motion is realized according to classical dynamics with the help of Large-scale Atomic Molecular Massively Parallel Simulator (LAMMPS) by the following loop:

- (i) NPT simulations for a fixed P and T are performed during the time interval  $\Delta t$ . The relative change of the system volume,  $\eta^3 = V(\Delta t)/V(0)$ , in the CG trajectories is used to update all the CG coordinates:  $\mathbf{R}_K \to \mathbf{R}_K/\eta$ . After iteration of this correction converges, the averaged volume remains unchanged and equal to its unperturbed value,  $V(0) = L^3$ .
- (ii) At the end of the interval, the CG system is then back-mapped (according to Subsec. 3.3.1 or 3.4.1 for Schemes 1 or 2, respectively), and the FG particles locations are

momentarily recreated.

- (iii) According to the specified Scheme, the FG particles are then reassembled to new CG particles with the masses and radii specified in Subsec. 3.3.2 or 3.4.2,
- (iv) The integration of the CG particles now continues at step (i) and these steps loop until the system has reached the final integration time.

As the interval  $\Delta t$  is varied, the rate with which the FG particles exchange between CG particles drastically alters their apparent diffusion. Other macroscopic characteristics of the CG model —like pressure and temperature in our case— remain unaffected.

In typical CG schemes, once FG particles are associated with a CG particle, they remain associated (or attached) to it for the entirety of the simulation. In the iteration detailed here, the FG particles are exchanged at increments of  $\Delta t$  according to the schemes provided below. In the limit that  $\Delta t$  goes to infinity (or longer than the entire simulation time), the CG dynamics reverts to the usual form. Otherwise, the exchange allows for FG particles to hop between CG particles. If the FG particles are bonded together, then such an exchange would not occur at any time scale unless there is bond breaking. This is the reason why many CG representations need not include exchange.

In the present work, we are considering CG particles that consist of unbonded FG particles. The latter will diffuse and spread across the CG particles. The exchange in Scheme 1 of Subsec. 3.3 allows for particles to perform this spread, but recaptures them into ordered structures at periodic increments of  $\Delta t$ . The exchange in Scheme 2 of Subsec. 3.4 uses the expected diffusion rate of the FG particles to spread and overlap with neighboring CG particles without restructuring the positions of the CG particles. The FG particles are positioned into the corresponding CG particle according to the Boltzmann distribution, and the subsequent movements align accordingly. At the exchange, the number of released and gained FG particles by a given CG particle vary according to the stochastic placement of the FG particles. However, the average number of FG particles entering and exiting a given CG particle—and, thus, their fluxes—are the same which is a minimal requirement to satisfy

detailed balance. In subsection 3.5, we provide an argument justifying—but do not strictly prove—for how the exchange moves obey detailed balance generally.

#### 3.3 Scheme 1: Exchange

At the end of a CG step in which the particles are propagated according to the CG dynamics of Sec. 3.2, we perform an exchange of FG particles between CG particles. The exchange is performed by first back-mapping of the CG particles into FG particles, and then reorganizing them into new CG particles according to a specified CG procedure.

#### 3.3.1 Scheme 1: Back-mapping (fine graining)

In Scheme 1, the CG system is back-mapped to a FG representation according to the following algorithm:

- (i) A Voronoi tessellation is constructed such that the current positions of the CG particles function as the centers of the Voronoi polyhedra. This tessellation completely covers the volume of the periodic box. <sup>37,40</sup>
- (ii) The FG particles known to be associated with a given CG particle are then released within their corresponding Voronoi polyhedron by implementing the Widom particle insertion method over the entire space of the associated polyhedron. As the union of these polyhedra is the entire volume, this action reinstates a statistically compatible thermalized configuration of the FG structure. Consequently, each FG particle has its own identity at a position that is no longer fixed to a prior CG particle, and it is now amenable to be coarse-grained in the next step.

#### 3.3.2 Scheme 1: Coarse graining

Given an arbitrary FG system, such as the one constructed using the back-mapping of Subsec. 3.3.1, we can construct a CG system by placing the would-be CG particles into a uniform ordered array. Specifically,  $N_{cg} = 6^3 = 216$  reference points at the coordinates

 $\{\mathbf{R}_K\}\ (K=1..N_{\rm cg})$  are chosen such that they form a simple cubic structure, each small cube having a size of  $l=L/N_{\rm cg}^{1/3}$ . The FG particles are assigned to a given CG particle as follows:

- (i) All N FG particles are grouped within the small cubes. If a cube does not contain any FG particles, it is eliminated from consideration, so that the resulting number  $N_{\rm cg}$  of CG cubes may be less than its initially defined value. If a cube contains only one FG particle, this single particle is allowed to move freely among other CG particles, representing its own CG type.
- (ii) The whole periodic box is then partitioned into  $N_{\text{cg}}$  non-empty Voronoi cells around the points  $\{\mathbf{R}_K\}$ . The identity of the FG particles associated with a CG particle for each of the Voronoi cells is tracked through the sets  $S_K$ .
- (iii) The mass of the resulting CG particles have a mass that is determined by the total number of FG particles pertaining to its Voronoi cell through Eq. (10). Their radii is initially set to that of the radius of gyration of the FG particles that are associated with it. For, example, the K-th CG particle has the radius

$$\rho_K = \sqrt{\frac{1}{N_K} \sum_{i \in S_K} (\mathbf{r}_i - \mathbf{R}_K)^2} , \qquad (11)$$

where  $N_K$  is the number of FG particles associated with the K-th CG particle that is initially located at the center of the K-th Voronoi cell and  $\mathbf{r}_i$  is the location of the i-th FG particle.

Thus the new CG particles have mass  $m_K$  and radius  $\sigma/2$  and are located at the centers of the cubic Voronoi tessellation at the end of each exchange. The initial momentum of each such particle is equal to the total momentum of all the FG particles in the Voronoi cell assigned to it.

# 3.4 Scheme 2: Exchange

In Scheme 2, we perform the exchange by back-mapping the FG particles and regrouping them through a slightly different procedure than performed in Scheme 1 in order to better preserve the dynamics of the CG particles by avoiding the periodic reconstruction of an ordered array of such particles.

#### 3.4.1 Scheme 2: Back-mapping

To incorporate the diffusion of the FG particles, they are released from the CG particles into regions associated with the motion and swelling of the Voronoi polyhedra that were attached to the CG particles at the beginning of a CG propagation step. At the end of that step, we now associate polyhedra that are centered at the CG particles but are swollen by a factor  $\alpha > 1$  related to the diffusive spread of the FG particles. For simplicity, we set this ratio such that it is

$$\alpha \equiv \frac{l'}{l} = \sqrt{1 + \frac{6D\Delta t}{l^2}} \,. \tag{12}$$

where l is the characteristic size of the initial Voronoi polyhedra defined earlier, and l' is the characteristic size of the swollen polyhedra at the end of the propagation. As in Scheme 1, the FG particles in set  $S_K$  are then released with the help of the Widom insertion method into the swollen polyhedra centered at the position of the associated k-th CG particle.

#### 3.4.2 Scheme 2: Coarse graining

The FG particles are then associated with CG particles. Unlike in Scheme 1, this is not done by means of an ordered array. Instead, the CG particles are in the same positions as the ones prior to the exchange. As the FG particles have spread across the boundaries of the instantaneous Voronoi polyhedra (following the scheme of Subsec 3.4.1), they can now be reassociated with the nearest CG particle and their associated Voronoi polyhedra.

For simplicity, the radii of the CG particles are, however, reset to be equal to the value corresponding to an averaged one of all the hydrodynamic radii, Eq. (11):

$$\bar{\rho} = \langle \rho_K \rangle$$
 (13)

The molecular dynamics (MD) simulations are performed with the spherical particles having mass  $M_K$  (Eq. (10)) and interacting with the WCA<sup>35</sup>-like PE (9) with  $\sigma = 2\bar{\rho}$ .

#### 3.5 Detailed Balance in the Exchange Schemes

The exchange schemes described above are shown here to satisfy detailed balance—namely, that

$$N_I P_{I \to J} = N_J P_{J \to I} \tag{14}$$

between any two neighboring CG particles where  $N_I$  is the number of FG particles contained in the  $I^{\text{th}}$  CG particle, and  $P_{I \to J}$  is the rate of FG particles going from the  $I^{\text{th}}$  to  $J^{\text{th}}$  CG particle—if averaged over sufficient time. We provide a proof of this claim below, but a proof of the conjecture for more general cases will need to be addressed in future work.

We start by noting that in either of the exchange schemes, the FG particles diffuse a typical distance s just before the back-mapping. We report below in Eq. (21) that this distance follows a linear scaling law— $s = \gamma l$  for some  $\gamma$ —with respect to the length l associated with the effective size of the Voronoi cell. Thus the new volume  $V + \Delta V$  which they then occupy is related to the volume V of the corresponding Voronoi cell, according to Eq. (12), as

$$(V + \Delta V)/V = (l'/l)^3 = \alpha^3,$$
 (15)

where  $\Delta V$  is the additional volume of the swollen Voronoi cell and  $\alpha$  is the ratio  $\frac{l'}{l}$ . The probability  $P_{\text{escape}}$  for leaving the Voronoi cell can be calculated as

$$P_{\text{escape}} = \Delta V / (V + \Delta V) = 1 - \alpha^{-3} = 1 - (1 + \gamma^2)^{-3/2}$$
 (16)

This probability is the same for all the Voronoi cells.

Given two adjacent CG particles I and J, the transition probability  $P_{I\to J}$  from the  $I^{\text{th}}$  to  $J^{\text{th}}$  Voronoi cell—viz CG particle—can be calculated by finding the volume  $\delta v_I$  which after

the swelling of cell I is contained within the  $J^{\text{th}}$  Voronoi polyhedron:

$$P_{I \to J} = P_{\text{escape}} \, \delta v_I / \Delta V_I \,, \tag{17}$$

where  $\Delta V_I$  is the additional volume of cell I. Similarly,

$$P_{J \to I} = P_{\text{escape}} \, \delta v_J / \Delta V_J \,. \tag{18}$$

Since for small intervals  $\Delta t$  (resulting from small probabilities  $P_{\text{escape}}$ ), the volumes  $\delta v_K$  do not depend on K, we obtain

$$\Delta V_I \cdot P_{I \to J} = \Delta V_J \cdot P_{J \to I} \ . \tag{19}$$

Meanwhile, the ratio of the volumes,  $\frac{\Delta V_K}{/}V_K = \alpha^3 - 1$ , as obtained form Eq. (15), is the same for all the Voronoi cells. Thus

$$V_I \cdot P_{I \to J} = V_J \cdot P_{J \to I} , \qquad (20)$$

and when multiplied by the density of the FG particles, it reduces to the detailed balance equation (14).

## 4 Results and Discussion

To reveal the effects of exchange in the hybrid CG dynamics outlined in Sec. 3, we examine the multiscale dynamics of an argon system under near supercritical conditions using the HS and LJ FG models detailed in Sec. 2.1. Thermodynamic consistency across the FG and CG scales with respect to pressure and temperature is retained by attaching standard numerical thermostats and barostats. We find that the value of the CG propagation time interval  $\Delta t$  between exchanges in the hybrid CG dynamics significantly affects the effective diffusion

coefficient  $D_{\text{eff}}$ . Specifically, the slope of the mean square displacement (MSD) of argon atoms shown in Fig. 3 varies dramatically with the choice of  $\Delta t$ . The CG particles in a pure CG propagation (when  $\Delta t \to \infty$ ) appear to be too slow. The periodic exchanges of the hybrid CG model manifests itself through the appearance of steps in the MSD trajectory. The horizontal plateaus of these steps correspond to the slow motion of the CG particles when the identities of separate FG atoms cannot be resolved. The vertical bars indicate the changes in the coordinates of the FG particles upon the statistical release of the particles through the back-mapping step in the exchange. With increasing exchange frequency, the MSD curves become steeper and the observed diffusion rate increases.

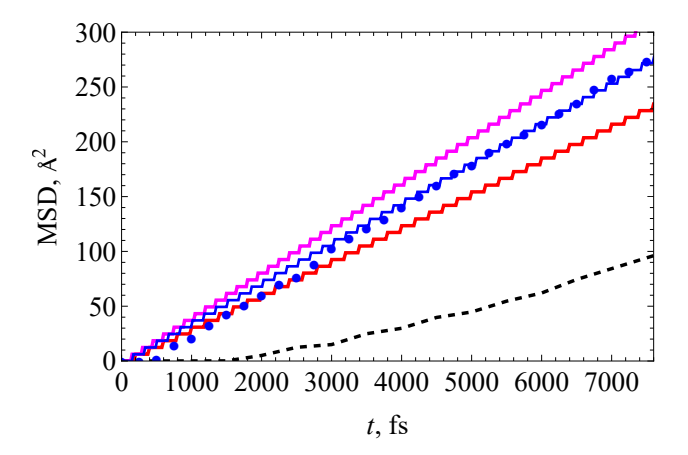


Figure 3: The MSD of the LJ particles obtained from the AA simulations (blue circles), pure CG Scheme 1 (dashed black curve) and its complementary hybrid scheme at  $\Delta t = 200$  fs (stepped red line),  $\Delta t = 169.04$  fs (stepped blue line) and  $\Delta t = 150$  fs (stepped magenta line). Other parameters: L = 40 Å ( $\phi = 0.351$ ), T = 300 K.

For both FG systems—that is HS and LJ,—we determined the dependence of  $D_{\rm eff}$  on  $\Delta t$  for each value of the volume fraction and temperature using Schemes 1 and 2 in the CG hybrid dynamics. (Refer to Figs. S1 and S2 in the Supporting Information (SI) for the full findings.) The values of  $\Delta t$  at which  $D_{\rm eff} = D$  is most optimal occur when the actual diffusion rate is reproduced by the hybrid simulations. The optimal values of  $\Delta t$  are listed in Table 1 and displayed in Figure 4.

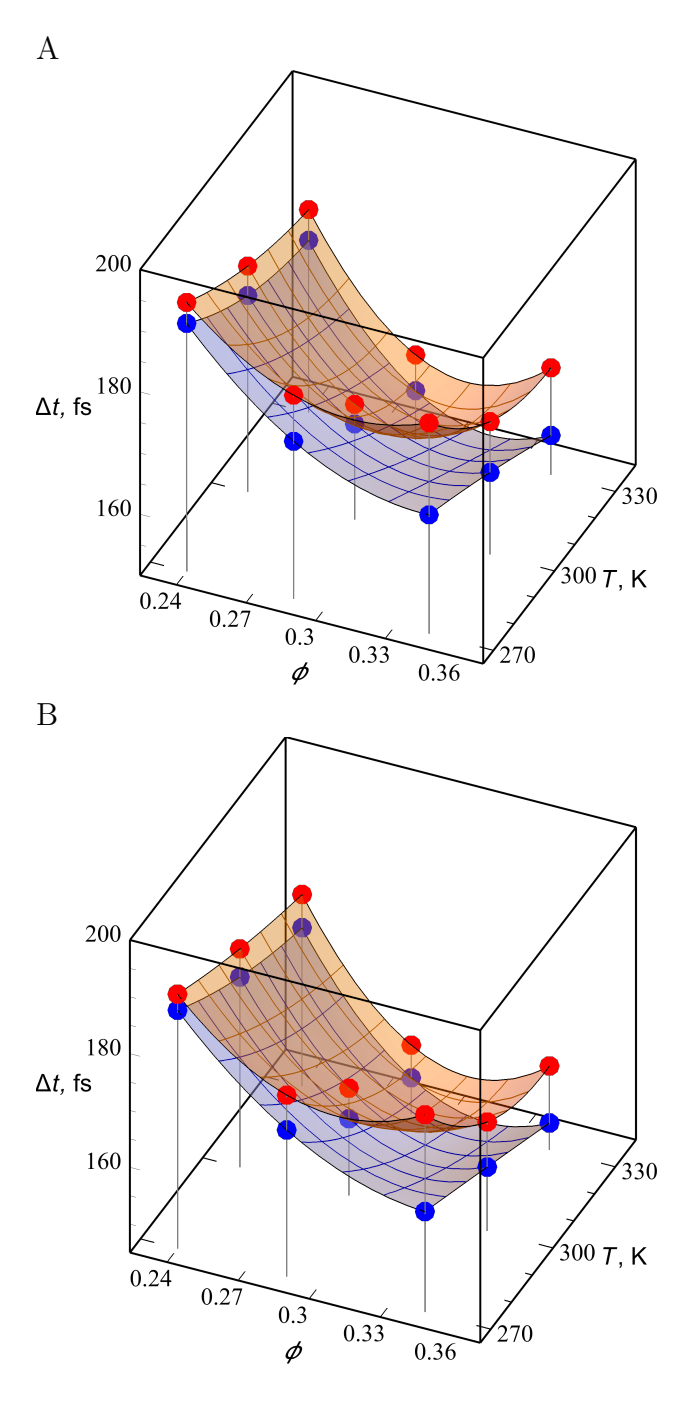


Figure 4: The optimized values of  $\Delta t$  at which hybrid simulations reproduce the diffusion coefficients of the AA simulations for (A) Scheme 1 and (B) Scheme 2. The color scheme is the same as in Fig. 1.

Table 1: The optimized values of  $\Delta t$  at which hybrid simulations reproduce the diffusion coefficients of the AA simulations.

			$\Delta t$ , fs (Scheme 1)		$\Delta t$ , fs (Scheme 2)	
L, Å	$\phi$	T, K	HS	LJ	HS	LJ
		270	184.50	169.45	179.75	162.70
40	0.351	300	171.71	163.39	164.19	156.26
		330	167.52	156.46	159.76	149.72
		270	183.31	175.78	176.94	170.81
42.5	0.292	300	168.83	165.62	163.87	158.48
		330	163.92	158.08	157.15	151.41
		270	194.01	190.57	189.77	186.94
45	0.246	300	186.95	182.14	183.44	178.49
		330	183.20	178.18	178.74	172.88

The characteristic path length for argon atoms during time  $\Delta t$  can be calculated as

$$s = \sqrt{6D\Delta t} \,. \tag{21}$$

The dependence of this length on the effective size of a Voronoi cell,  $l = L/N_{\text{cg}}^{1/3} = L/6$ , at different values of the temperature is shown in Fig. 5 for both schemes (see also Fig. S3 in the SI). Interestingly, this dependence is well described by the linear fit

$$s = \gamma \cdot l \,, \tag{22}$$

where the values of  $\gamma$  are 0.374 for Scheme 1 and 0.368 for Scheme 2. This finding confirms that the optimal time  $\Delta t$  needed to mimic the AA diffusion within the hybrid CG simulations corresponds to the duration of time necessary for the atoms to be exchanged between adjacent Voronoi cells, regardless to the actual system (HS or LJ in our case), its state and the scheme used.

In Figures 6 and 7, the effective diffusion coefficient,  $D_{\rm eff}$ , of the FG particles obtained from the CG hybrid simulations (using several representative values of  $\Delta t$ ) is benchmarked against the diffusion coefficients of the pure CG (when  $\Delta t$  is infinity) and the underlying

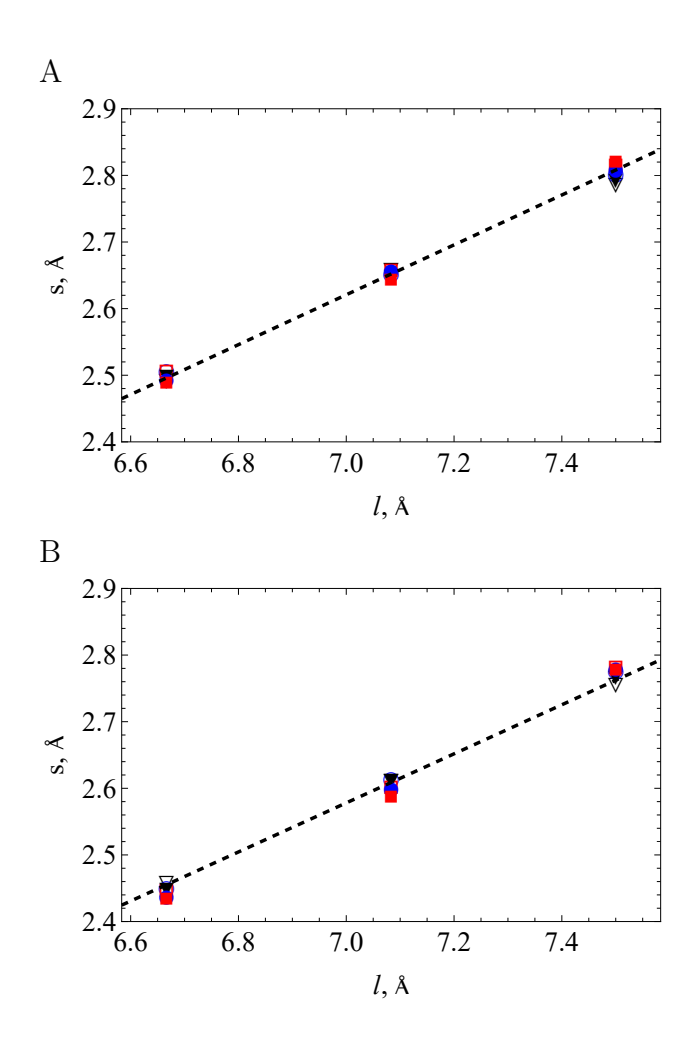


Figure 5: Characteristic path length, Eq. (21), of argon atoms as a function of effective size of a Voronoi cell for HS (open symbols) and LJ (filled symbols) systems for (A) Scheme 1 and (B) Scheme 2 at different temperatures:  $T=270~\mathrm{K}$  (triangles),  $T=300~\mathrm{K}$  (circles) and  $T=330~\mathrm{K}$  (squares). The dashed line is the linear regression fit, Eq. (22).

AA FG system. The diffusion is not the same between the pure CG and AA systems thus providing evidence for the need for the exchange mechanism that has been argued in this work. Meanwhile, the diffusion constant of the AA systems is bounded by the CG hybrid simulations with exchange times between 150 to 200 fs. While the agreement is not exact, presumably because of the approximations inherent in the selected exchange schemes, this suggests the need for the inclusion of an exchange mechanism in coarse-graining unbonded particles.

#### 5 Conclusions

In this paper, we demonstrated the need for including an exchange term in CG approaches so as to account for the associativity of the particles that underlies representativity. To our knowledge, the exchange mechanism has not been accounted for in prior approaches aimed at obtaining dynamical consistency between FG and CG scales.

We introduced two possible algorithms for carrying out the exchange of FG particles associated with a given CG particle. In both algorithms, CG particles are propagated by the CG dynamics and the exchange takes place at regular (or periodic) time intervals at the characteristic exchange time. In the first scheme, the CG particles are back-mapped to FG particles at statistically consistent positions and momenta within the Voronoi polyhedron of each CG particle, and are subsequently coarse-grained onto a grid of uniform CG solvent particles. In the second scheme, the FG particles are back-mapped to positions and momenta statistically consistent with the overlapping Voronoi polyhedra that have been enlarged due to the diffusion, and are subsequently coarse-grained by association with the standard Voronoi polyhedron of a given CG particle. Both schemes lead to dynamical consistency in the diffusion of the FG particles, but the second scheme has the advantage that it does not introduce an arbitrary regularization of the structure of the CG particles at the characteristic exchange times. As a consequence, the second scheme provided structural

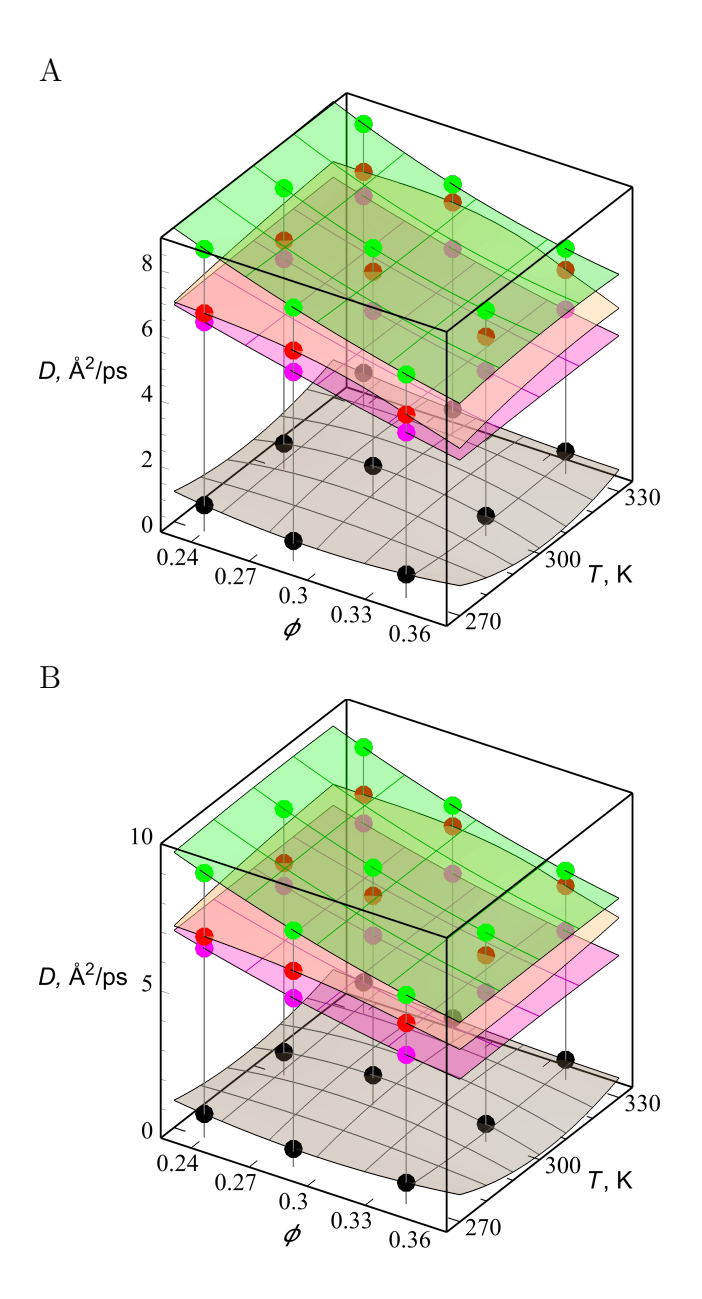


Figure 6: The effective diffusion  $D_{\rm eff}$  for Scheme 1 as a function of  $\phi$  and T at different values of  $\Delta t$  for the (A) HS and (B) LJ systems:  $\Delta t = \infty$ , i.e., pure CG system (black dots and gray interpolating surface),  $\Delta t = 200$  fs (magenta dots and interpolating surface),  $\Delta t = 150$  fs (green dots and interpolating surface), and D for AA HS system (red dots and light red interpolating surface).

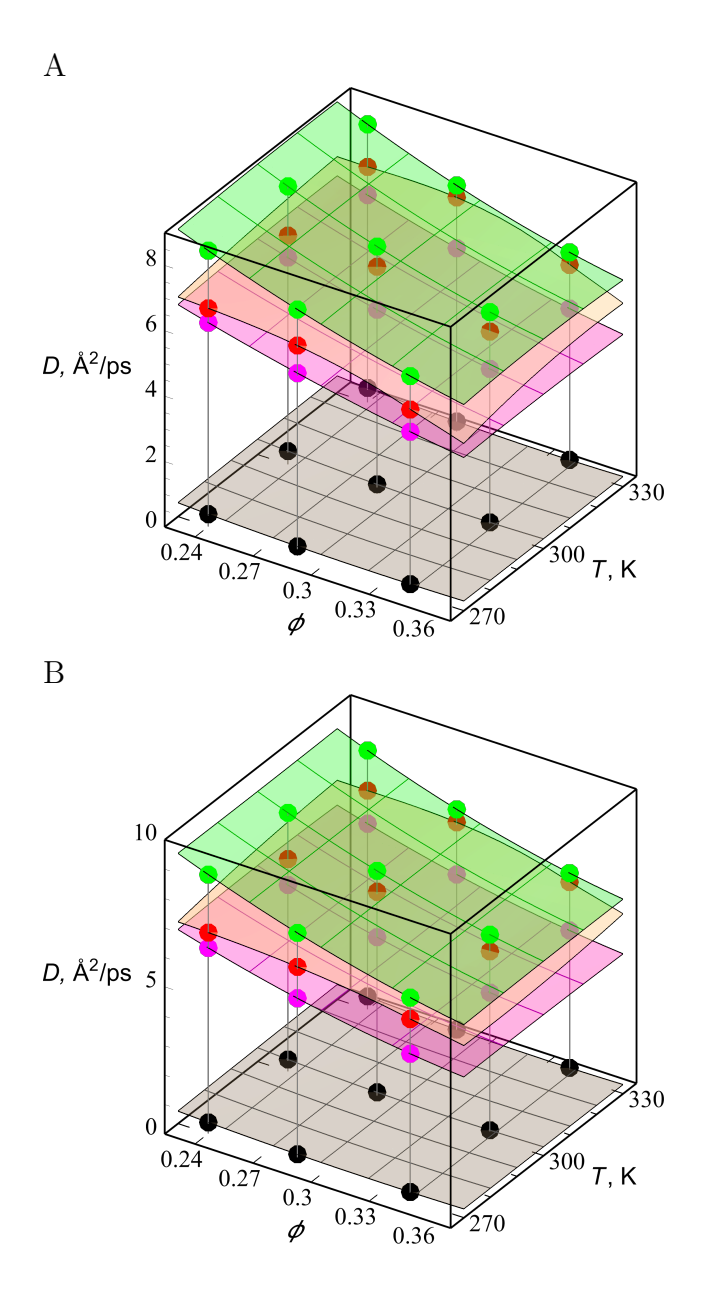


Figure 7: The effective diffusion  $D_{\rm eff}$  for Scheme 2 as a function of  $\phi$  and T at different values of  $\Delta t$  for the (A) HS and (B) LJ systems. Other parameters and the color scheme are the same as in Fig. 6.

consistency as well as dynamical consistency.

We demonstrated the efficacy of the schemes through simulations of supercritical argon in the isothermal-isobaric ensemble. Retaining the association (and diffusion) of the individual atoms through the CG particles allows us to simulate the fluid phase dynamics of argon with the correct dissipative properties. Without our exchange schemes, the standard coarse-graining of the system would restrict particle mobility by assigning them to a fixed dissipative particle, and thus limit their diffusion. Instead, the exchange schemes allow for the spread of the FG particles and the correct match to the FG dynamics without necessitating an artificially large acceleration of the CG particles in the standard schemes. Thus, through the introduction of an exchange scheme, we addressed both the issues of representability and the coarse-graining of time scales in a supercritical argon fluid when more than one atom is associated with a given CG particle.

We anticipate that the implementation of dynamical consistency in increasingly large coarse-grain systems will necessarily need to account for molecules that are not chemically bonded to each other. Even a system which allocates more than one water particle to a coarse-grained particle will necessarily be affected by the lack of exchange of waters between the coarse-grained particles. Thus an accounting of the exchange between coarse-grained particles is essential to their representation, and in turn to the degree to which dynamical consistency is satisfied. In the present work we have suggested a pair of models that provide for exchange in the representation of coarse-grained particles. Future work will include providing a firmer bottom-up footing for these models—by e.g., generalizing the degree to which it satisfies detailed balance and other thermodynamic constrains,—layering the exchange contribution to other coarse-grained methods, and applying them to characterize chemical dynamics in large heterogeneous solvents.

# 6 Supporting Information for Publication

The SI available for this publication contains three figures: Figures S1 and S2 provide comparisons of time-dependent diffusion determined by Schemes 1 and 2, respectively, between the HS and LJ systems across several system conditions. Figure S3 redraws the data shown in Fig. 5 in three dimensions to emphasize the apparent linear dependence of the characteristic path length on the effective size of a Voronoi cell, as well as its insensitivity to the temperature.

# Acknowledgement

RH had the great fortune to have been a postdoctoral student with Gregory "Greg" A. Voth. We are happy to dedicate this work in honor of his current and future work through this contribution to the Festschrift celebrating his 65<sup>th</sup> birthday. This work has been partially supported by the National Science Foundation (NSF) through Grant No. CHE 2102455. The computing resources necessary for this work were provided, in part, through allocation CTS090079 from the Advanced Cyberinfrastructure Coordination Ecosystem: Services & Support (ACCESS) program, which is supported by National Science Foundation (NSF) grants #2138259, #2138286, #2138307, #2137603, and #2138296.

## References

- (1) Akkermans, R. L. C.; Briels, W. J. Coarse-Grained Dynamics of One Chain in a Polymer Melt. J. Chem. Phys. 2000, 113, 6409, DOI: 10.1063/1.1308513.
- (2) Lyubartsev, A. P.; Karttunen, M.; Vattulainen, I.; Laaksonen, A. On Coarse-Graining by the Inverse Monte Carlo Method: Dissipative Particle Dynamics Simulations Made to a Precise Tool in Soft Matter Modeling. Soft Matter 2002, 1, 121–137, DOI: 10. 1081/SMTS-120016746.

- (3) Padding, J. T.; Briels, W. J. Time and Length Scales of Polymer Melts Studied by Coarse-Grained Molecular Dynamics Simulations. J. Chem. Phys. 2002, 117, 925, DOI: 10.1063/1.1481859.
- (4) Müller-Plathe, F. Coarse-Graining in Polymer Simulation: From the Atomistic to the Mesoscopic Scale and Back. *ChemPhysChem* **2002**, *3*, 754–769, DOI: 10.1002/1439-7641(20020916)3:9<754::AID-CPHC754>3.0.CO;2-U.
- (5) Depa, P.; Maranas, J. Speed up of Dynamic Observables in Coarse-Grained Molecular-Dynamics Simulations of Unentangled Polymers. J. Chem. Phys. 2005, 123, 094901, DOI: 10.1063/1.1997150.
- (6) Izvekov, S.; Voth, G. A. Modeling Real Dynamics in the Coarse-Grained Representation of Condensed Phase Systems. J. Chem. Phys. 2006, 125, 151101, DOI: 10.1063/1. 2360580.
- (7) Marrink, S. J.; Risselada, H. J.; Yefimov, S.; Tieleman, D. P.; de Vries, A. H. The MARTINI Force Field: Coarse Grained Model for Biomolecular Simulations. J. Phys. Chem. B 2007, 111, 7812–7824, DOI: 10.1021/jp071097f.
- (8) Karimi-Varzaneh, H. A.; Carbone, P.; Müller-Plathe, F. Fast Dynamics in Coarse-Grained Polymer Models: The Effect of the Hydrogen Bonds. J. Chem. Phys. 2008, 129, 154904.
- (9) Harmandaris, V.; Kremer, K. Predicting Polymer Dynamics at Multiple Length and Time Scales. Soft Matter 2009, 5, 3920–3926, DOI: 10.1039/B905361A.
- (10) Molinero, V.; Moore, E. B. Water Modeled As an Intermediate Element Between Carbon and Silicon. J. Phys. Chem. B 2009, 113, 4008–4016, DOI: 10.1021/jp805227c.
- (11) Armstrong, J. A.; Chakravarty, C.; Ballone, P. Statistical Mechanics of Coarse Graining:

- Estimating Dynamical Speedups from Excess Entropies. J. Chem. Phys. 2012, 136, 124503, DOI: 10.1063/1.3697383.
- (12) Hagy, M. C.; Hernandez, R. Dynamical Simulation of Dipolar Janus Colloids: Dynamical Properties. J. Chem. Phys. 2013, 138, 184903, DOI: 10.1063/1.4803864.
- (13) Jin, J.; Schweizer, K. S.; Voth, G. A. Understanding Dynamics in Coarse-Grained Models. I. Universal Excess Entropy Scaling Relationship. J. Chem. Phys. 2023, 158, 034103, DOI: 10.1063/5.0116299.
- (14) Jin, J.; Schweizer, K. S.; Voth, G. A. Understanding Dynamics in Coarse-Grained Models. II. Coarse-Grained Diffusion Modeled Using Hard Sphere Theory. J. Chem. Phys. 2023, 158, 034104, DOI: 10.1063/5.0116300.
- (15) Li, Z.; Bian, X.; Li, X.; Karniadakis, G. E. Incorporation of Memory Effects in Coarse-Grained Modeling via the Mori-Zwanzig Formalism. J. Chem. Phys. 2015, 143, 243128, DOI: 10.1063/1.4935490.
- (16) Cui, Q.; Hernandez, R.; Mason, S. E.; Frauenheim, T.; Pedersen, J. A.; Geiger, F. Sustainable Nanotechnology: Opportunities and Challenges for Theoretical/Computational Studies. J. Phys. Chem. B 2016, 120, 7297–7306, DOI: 10.1021/acs.jpcb.6b03976.
- (17) Clark, A. E.; Adams, H.; Hernandez, R.; Krylov, A. I.; Niklasson, A. M. N.; Sarupria, S.; Wang, Y.; Wild, S. M.; Yang, Q. The Middle Science: Traversing Scale in Complex Many-Body Systems. ACS Cent. Sci. 2021, 7, 1271, DOI: 10.1021/acscentsci. 1c00685.
- (18) Füchslin, R. M.; Fellermann, H.; Eriksson, A.; Ziock, H.-J. Coarse Graining and Scaling in Dissipative Particle Dynamics. J. Chem. Phys. 2009, 130, 214102, DOI: 10.1063/ 1.3143976.

- (19) Han, Y.; Jin, J.; Voth, G. A. Constructing Many-Body Dissipative Particle Dynamics Models of Fluids from Bottom-Up Coarse-Graining. J. Chem. Phys. 2021, 154, 084122, DOI: 10.1063/5.0035184.
- (20) Reith, D.; Pütz, M.; Müller-Plathe, F. Deriving Effective Mesoscale Potentials from Atomistic Simulations. *J. Comput. Chem.* **2003**, *24*, 1624–1636, DOI: 10.1002/jcc. 10307.
- (21) Noid, W. G.; Chu, J.-W.; Ayton, G. S.; Krishna, V.; Izvekov, S.; Voth, G. A.; Das, A.; Andersen, H. C. The Multiscale Coarse-Graining Method. I. A Rigorous Bridge Between Atomistic and Coarse-Grained Models. J. Chem. Phys. 2008, 128, 244114, DOI: 10.1063/1.2938860.
- (22) Wang, H.; Junghans, C.; Kremer, K. Comparative Atomistic and Coarse-Grained Study of Water: What Do We Lose by Coarse-Graining? Eur. Phys. J. E 2009, 28, 221—-229, DOI: 10.1140/epje/i2008-10413-5.
- (23) Das, A.; Andersen, H. C. The Multiscale Coarse-Graining Method. IX. A General Method for Construction of Three Body Coarse-Grained Force Fields. J. Chem. Phys. 2012, 136, 194114, DOI: 10.1063/1.4705417.
- (24) Wagnera, J. W.; Damaa, J. F.; Durumeric, A. E. P.; Voth, G. A. On the Representability Problem and the Physical Meaning of Coarse-Grained Models. J. Chem. Phys. 2016, 145, 044108, DOI: 10.1063/1.4959168.
- (25) Shmilovich, K.; Stieffenhofer, M.; Charron, N. E.; Hoffmann, M. Temporally Coherent Backmapping of Molecular Trajectories From Coarse-Grained to Atomistic Resolution. J. Phys. Chem. A 2022, 126, 9124–9139, DOI: 10.1021/acs.jpca.2c07716.
- (26) Chennakesavalu, S.; Toomer, D. J.; Rotskoff, G. M. Ensuring Thermodynamic Consistency with Invertible Coarse-Graining. *J. Chem. Phys.* **2023**, *158*, 124126, DOI: 10.1063/5.0141888.

- (27) Johnson, M. E.; Head-Gordon, T.; Louis, A. A. Representability Problems for Coarse-Grained Water Potentials. J. Chem. Phys. 2007, 126, 144509, DOI: 10.1063/1. 2715953.
- (28) Han, Y.; Dama, J. F.; Voth, G. A. Mesoscopic Coarse-Grained Representations of Fluids Rigorously Derived from Atomistic Models. J. Chem. Phys. 2018, 149, 044104, DOI: 10.1063/1.5039738.
- (29) Chennamsetty, N.; Bock, H.; Gubbins, K. Coarse-Grained Potentials from Widom's Particle Insertion Method. Mol. Phys. 2005, 103, 3185–3193, DOI: 10.1080/ 00268970500208658.
- (30) Wilhelm, E. Thermodynamic properties of a hard sphere fluid with temperature dependent effective hard sphere diameter. *J. Chem. Phys.* **1974**, *60*, 3896–3900, DOI: 10.1063/1.1680836.
- (31) Heyes, D. M. Transport coefficients of Lennard-Jones fluids: A molecular-dynamics and effective-hard-sphere treatment. *Phys. Rev. B* **1988**, *37*, 5677–5696, DOI: 10. 1103/PhysRevB.37.5677.
- (32) Gilgen, R.; Kleinrahm, R.; Wagner, W. Measurement and correlation of the (pressure, density, temperature) relation of argon I. The homogeneous gas and liquid regions in the temperature range from 90 K to 340 K at pressures up to 12 MPa. *Journal of Chemical Thermodynamics* **1994**, *26*, 383–398, DOI: 10.1006/jcht.1994.1048.
- (33) Mulero, A., Ed. Theory and Simulation of Hard-Sphere Fluids and Related Systems; Lecture Notes in Physics; Springer Berlin, Heidelberg: Berlin, 2008; Vol. 753; DOI: 10.1007/978-3-540-78767-9.
- (34) Woodcock, L. V. Physical-constant equations-of-state for argon isotherms. *Int. J. Ther-mophysics.* **2019**, *40*, 65, DOI: 10.1007/s10765-019-2530-4.

- (35) Weeks, J. D.; Chandler, D.; Andersen, H. C. Role of Repulsive Forces in Determining the Equilibrium Structure of Simple Liquids. *J. Chem. Phys.* **1971**, *54*, 5237–5247, DOI: 10.1063/1.1674820.
- (36) Flekkøy, E. G.; Coveney, P. V. From Molecular Dynamics to Dissipative Particle Dynamics. *Phys. Rev. Lett.* **1999**, *83*, 1775–1778, DOI: 10.1103/PhysRevLett.83.1775.
- (37) Eriksson, A.; Jacobi, M. N.; Nyström, J.; Tunstrøm, K. On the microscopic foundation of dissipative particle dynamics. *Europhysics Letters* 2009, 86, 44001, DOI: 10.1209/ 0295-5075/86/44001.
- (38) Knight, C.; Voth, G. A. The Curious Case of the Hydrated Proton. *Acc. Chem. Res.* **2012**, *45*, 101–109, DOI: 10.1021/ar200140h.
- (39) Agmon, N.; Bakker, H. J.; Campen, R. K.; Henchman, R. H.; Pohl, P.; Roke, S.; Thämer, M.; Hassanali, A. Protons and Hydroxide Ions in Aqueous Systems. *Chem. Rev.* **2016**, *116*, 7642–7672, DOI: 10.1021/acs.chemrev.5b00736.
- (40) Flekkøy, E. G.; Coveney, P. V.; Fabritiis, G. D. Foundations of Dissipative Particle Dynamics. *Phys. Rev. E* **2000**, *62*, 2140–2157, DOI: 10.1103/PhysRevE.62.2140.
- (41) Widom, B. Some Topics in the Theory of Fluids. *J. Chem. Phys.* **1963**, *39*, 2808, DOI: 10.1063/1.1734110.
- (42) Widom, B. Random Sequential Addition of Hard Spheres to a Volume. J. Chem. Phys. 1966, 44, 3888–3894, DOI: 10.1063/1.1726548.

# TOC Graphic

